

Expanding and Self-Organizing 2D Universe Models Emerging from Frozen Trivalent Spin Networks

Christine C. Dantas

Divisão de Astrofísica (INPE-MCTI), Av. dos Astronautas, 1758, Jardim da Granja,
CEP: 12227-010, São José dos Campos, SP, Brazil

E-mail: `christine.dantas@inpe.br`

Abstract.

We revisit the topic of self-organized criticality (SOC) in simple statistical graph models, with the purpose of capturing essential processes leading to the emergence of macroscopic spacetime from the microscopic dynamics in loop quantum gravity (LQG). We performed a large set of simulations based on extensions of the frozen trivalent spin network (TSN) model explored previously by Ansari and Smolin. Their model mimicked the sandpile dynamics by the application of random vertex propagation rules in the TSN, leading to a SOC behavior in the distribution of the avalanche sizes, as well as a slowly expanding, 2-dimensional dual (triangulated) space. Here we show that a growth scheme for the stochastic, slow external driving force, differing from the classical sandpile model, also resulted in power-law distributed avalanche sizes. Our simulations also produced expanding dual spaces, with two basic classes of evolution: one with power-law correlations in “space” and “time”, and the other with “loitering” and exponential phases. Our work expands the range of models in which critical states in the TSN may lead to expansion effects in the dual space, without fine-tuning.

Keywords: loop quantum gravity; quantum cosmology; spin network model; self-organized critical phenomenon

1. Introduction

The expectation that physical interactions should be fundamentally unified around the Planck scale ($\ell_{\text{Pl}} \equiv \sqrt{G\hbar/c^3} \sim 10^{-33}$ cm), as well as the presence of singularities in general relativity, suggest that gravity should be quantized. Although a theory of quantum gravity has not been established yet, there has been robust developments in the past decades, based on distinct motivations and approaches. These can be roughly traced back from two fronts [1]: the particle physics community (unification of interactions), and the general relativity community (breakdown of the smooth, classical spacetime). In the latter front, developments like Loop Quantum Gravity (LQG) [2] [3] [4] incorporate a relational, background independent framework at its foundation [5], leading to the prospect of a non-perturbative canonical quantization of general relativity.

Abstract graphs were first envisioned by R. Penrose as a possible model of spacetime geometry [6]. Graphs are represented in LQG in terms of spin networks, roughly defined as follows [7], [4]. A spin network state is expressed in terms of a graph, γ , embedded in a spatial manifold Σ ; the graph is composed of a finite number of vertices (or nodes) and incident edges. The edges are labelled by an irreducible representation of $\text{SU}(2)$, namely, spins j_k , whereas vertices are labelled by intertwining operators (based on the tensor product of the representations carried by the incoming and outgoing edges). The physical interpretation is that each node inside an elementary region of Σ contributes a quanta of volume, whereas each edge crossing the corresponding surface of the region contributes a quanta of area, being therefore quantum states of space.

Spin network states form a basis, at the kinematical level, for the representative quantum state functions of 3-dim space. Physical states would arise from the solution of the Hamiltonian constraints, which generate the dynamics [3]. Quantum dynamics is one of the main unsolved problems in LQG. One possibility was based on the concept of “sum-over-histories”, inspired by Feynman’s functional integral quantization scheme, the so-called “spin-foam models” [8]. A complete knowledge of the evolution of gravitational quantum states as well as the retrieval of Einstein’s equations in the continuum limit of LQG are the main open problems of the theory [1],[2],[4].

One intriguing idea, proposed initially by Markopoulou and Smolin [9], was the possibility that the underlying quantum spacetime could present critical behavior, analogous to a self-organized critical (SOC) phenomena [10], [11], [12], [13], [14], resulting in the possible emergence of classical spacetime from such a process. Furthermore, if the discrete structure of spacetime in the Planck regime is a SOC system, then it would be an interesting possibility that the classical spacetime limit would require no fine-tuning to be achieved. Note also that this idea arises as an alternative approach to the problem of the action of the Hamiltonian constraint in LQG [1], [2], [4], in which one looks for consistent rules for the evolution of the kinematic states leading to a possible recovery of the action of that constraint in the classical limit.

That idea was investigated by Borissov and Gupta [15], in context of the so-called “frozen” *trivalent spin networks* (TSN). They devised a random edge model with specific

propagation rules (avalanches of edge color updates after a perturbation of the system), so that it generated a dynamics in which the system evolved to gauge invariant states after every avalanche. Their results, however, did not produce a critical behavior (i. e., a power-law distribution of avalanches) in the TSN. Subsequently, Ansari and Smolin [16] (hereon [Ans08]) revisited the problem in the same frozen TSN context but using a random vertex model, founding evidence for SOC behavior. Chen and Zhu [17] (hereon [Che08]) extended the random edge model of Borissov and Gupta, by including a probability distribution for the edge color propagation, as well as considering a non-fixed value for the color change, founding SOC behaviors for this model, but not in the random vertex model (by the application of their proposed model extension), differing therefore from the results by [Ans08] under simpler conditions.

The main question addressed in our paper is whether it is possible to obtain expanding universe models at higher rates than in previous works, but still producing SOC behavior. In order to investigate this possibility, we adopted a growth scheme for the externally driving perturbations (therefore differing from a simple sandpile model, in which the perturbation is always set to be a fixed, small scale one). We revisited the model by [Ans08], combining it with more flexible values for the edge color updates, somewhat similarly to [Che08], but here implementing a growth scheme (using 3 different models), which has not been explored previously.

Our paper is organized as follows. In Sec. 2, we review the frozen TSN model, and summarize the main concepts of SOC. In Sec. 3, we introduce the models and simulations, as well as a possible interpretation of dynamics (i.e., time evolution) in these models. In Sec. 4, we present our results, which are summarized and discussed in Sec. 5. The Appendix A presents supplementary results on the simulations executed for the smaller TSN.

2. The frozen TSN model and SOC

2.1. Description of the TSN, propagation rules, and previous results.

A spin network can be modelled as a labelled graph, γ , with N_v number of vertices (nodes), so that each of its vertices, v_i ($i = 1, \dots, N_v$), has a certain number of oriented edges e_1, \dots, e_m . These edges are labelled by the irreducible representation of the SU(2) group in $(3 + 1)$ -dim LQG, that is, in terms of spins, j_β , or colors, given by $c_\beta = 2j_\beta$.

Following [Ans08], we study open, 2-dim trivalent ($m = 3$) spin networks (TSN), so that the dual space to the TSN is a (planar) triangulation of a region of space. The physical length of a side of the triangle is given by $l_\beta \sim (1/2)c_\beta l_{\text{Planck}}$. The gauge-invariance constraint on any given vertex v_i , with edge colors ($c_1 = a, c_2 = b, c_3 = c$), is given by:

$$a + b \geq c; \quad a + c \geq b; \quad b + c \geq a; \tag{1}$$

$$a + b + c = \text{even}. \tag{2}$$

In [Ans08], the proposed propagation rules for the evolution of spin network states was given by simultaneously adding or subtracting a fixed color on all edges belonging to a given vertex. Specifically, the algorithm was the following:

- (i) Initialize the TSN by labelling each edge by a random color, so that the gauge conditions (Eqs. 1 and 2) are satisfied at each vertex in whole TSN. In [Ans08], the initial colors were randomly chosen from integers $\mathbf{C}_{\text{init}} = \{10, \dots, 20\}$ (even).
- (ii) Choose a random (activating) vertex upon which the external driving disturbance will act, by subtracting a color disturbance, $\Delta c = 2$, from all its edges. If at least one of the edges is 0, do not act and choose another vertex.
- (iii) Test for the gauge conditions (Eqs. 1 and 2) by sweeping the TSN with a fixed ordering. In [Ans08], this ordering was: left to right and top to bottom.
- (iv) For each gauge non-invariant (GNI) vertex, add the color disturbance $\Delta c = 2$ to each of its edges.
- (v) Repeat (iii) until the TSN is completely gauge-invariant again. The size of the avalanche is given by the number of updates (color additions) imposed on the vertices (repeated vertices are counted). The area of the avalanche is given by the number of individual vertices involved in the avalanche (not counting how many times they eventually were updated in the same avalanche).
- (vi) Go to item (ii) and repeat the procedure, updating the *step counter*, k .

In [Ans08], the simultaneous addition of a color to the edge colors of a GNI-vertex was fixed to $\Delta c = 2$, throughout the evolution. This fixed scheme produced a SOC behavior with a tendency for the average TSN color to increase as a function of steps, although in a highly oscillatory manner, probably due to the size of the TSN used, as pointed out by [Che08]. The latter authors revisited the matter using a different prescription, in which Δc was not fixed, but randomly chosen between 2 and a maximum color value (even integers), ranging from values in the set: $c_{\text{max}} = \{10, 30, 100, 1000, 10000\}$. They also used a larger number of vertices, with a probability scheme for color propagation. They found that the average color increased linearly after an initial relaxation period.

2.2. Self-organized criticality.

In the late 80s, a new unifying theory explaining the nature of power-law relations arising in complex systems was proposed by Bak et al.[10], [11], which subsequently received considerable attention (e.g., [12], [13], [14], and references therein). The basic features of this theory, named *self-organized criticality* (SOC), is best understood in terms of the simple dynamics of sandpiles (the first model exemplifying how a system moves to its critical state without any fine-tuning of an external parameter).

Generally, from an arbitrary initial condition (e.g., a sandpile) and a stochastic evolution, the system reaches a critical state after a sufficient long time, characterized by power-law correlations in space and time. This can be seen in the sandpile model by

dropping a grain of sand at arbitrary times and locations on the sandpile, so that an amount of grains of sand may topple down according to certain critical value at each site – creating a finite avalanche, until equilibrium is again reached.

For the SOC phenomena, a power-law probability distribution of *avalanche size* (s) is expected (also known as the *Pareto distribution function*, c.f. [13]):

$$\mathcal{P}(s) = s^\alpha, \quad \alpha < 0. \quad (3)$$

There are theoretical open questions and new interpretations, specially resulting from the considerable advancement of this field (and from highly heterogeneous applications), which can be found, e.g., in the critical review of Ref. [14]. However, there are generally accepted typical features shared by SOC systems, such as a slow external driving perturbation and fast relaxation, so that the driving force does not disturb the running of the avalanche, while it is occurring. Indeed, as it is clear from the propagation rules presented in Sec. 2, the TSN is randomly disturbed only after it regains a gauge-invariant state. Hence, in the present case, by design, relaxation triggered by a color avalanche is always faster than the interval between external driving perturbations. This feature is preserved in our new models, to be described in the next section.

3. New propagation rules with a growth scheme for the frozen TSN model

The motivation to explore a growth scheme comes from the observation in [Ans08] and [Che08] that the dual space tends to expand due to an overall increase of the mean color of the TSN, as a function of the number of steps. The question we address here is whether expanding models at higher rates than those reported previously still produce SOC behavior. In this section, we describe our models in detail.

3.1. New models.

We adopt of a growth scheme for the color disturbance Δc , by redefining it through the addition of some fixed or variable quantity \mathcal{C} , or of a related function of the *step counter*, k ($k = 1, \dots, N_{\text{steps}}$). Hence, only the steps (ii) and (iv) in the propagation rules (c.f. Sec. 2) are affected by this scheme. All models start with an initial $\Delta c_{k=1} = 2$. We describe our models as follows.

3.1.1. Model A: This model represents a simple extension in which a fixed incremental color \mathcal{C}_A is added at each step counter k to the color disturbance Δc . The color addition scheme is given by:

$$\Delta c_{k+1} = \Delta c_k + \mathcal{C}_A, \quad (4)$$

where we analysed the set $\mathcal{C}_A = \{2, 20, 200\}$ (for each run). For example, for $\mathcal{C}_A = 2$: $\Delta c_{k=1} = 2, \Delta c_{k=2} = 4, \Delta c_{k=3} = 6, \dots$, etc; for $\mathcal{C}_A = 20$: $\Delta c_{k=1} = 2, \Delta c_{k=2} = 22, \Delta c_{k=3} = 42, \dots$, etc..

3.1.2. Model B: This model modifies the random scheme of [Che08], with a color addition given by:

$$\Delta c_{k+1} = \Delta c_k + \text{Rand}(2, \mathcal{C}_B), \quad (5)$$

with $\mathcal{C}_B = \{4, 20, 200\}$. Rand is a random generator of even integers in the indicated interval (inclusive), updated at each step. For instance, for $\mathcal{C}_B = 20$, we could have $\Delta c_{k=1} = 2, \Delta c_{k=2} = 14$ (for Rand = 12), $\Delta c_{k=3} = 22$ (for Rand = 8), ..., etc.

3.1.3. Model C: This model uses a conditional exponential increase of color addition, as a function of the activation step k . The color addition scheme is given by:

$$\Delta c_{k+1} = \Delta c_k + \mathcal{C}_C[f(k)], \quad (6)$$

where

$$\mathcal{C}_C[f(k)] = \begin{cases} \{2, 20, 200\}, & \text{if } f(k) \equiv \exp(10k/N_{\text{steps}}) > \Delta c_k; \\ 0, & \text{otherwise.} \end{cases} \quad (7)$$

Note that this model incorporates an exponential behavior modulated by a step function, mimicking the effect of some critical condition on the driving perturbation, which is activated as function of an external time.

3.1.4. Model Ans08: We also reproduce the results by [Ans08] [16]. For this model, we ran a set of simulations using different numbers of steps and a somewhat larger number of vertices in the TSN, but with their same propagation rules. These simulations are useful as a reference for our code implementation and for comparison purposes.

3.2. A note on dynamics and time.

Before describing our simulations, we briefly digress to qualitatively motivate our growth scheme of perturbations. The problem of time in the context of canonical quantization of general relativity is a difficult one [18]. In the present case, the rules described in the previous section lead to the evolution the TSN from a gauge invariant state to another gauge invariant state, considering the intermediary propagation of edge colors from the random vertices disturbances. Hence, the steps counter, k , inherent to the process of vertex activation and color propagation, can be regarded as “time-keeping” device, i.e., an external variable parameterizing the agency of sequential, stochastic disturbances on vertices and their subsequent excitations.

There is a sense in which those state-to-state changes could be associated with a (at least, partial) order process, akin to a “temporal” progression, if we consider that the externally induced disturbances are driven from an orderly (i.e., a sequentially labelable) process arising from a external reservoir. Although we do not attribute any physical specification for such a reservoir, in more realistic scenarios in which the TSN can be enlarged or be part of an ensemble of interacting TSNs, it is reasonable to assume that such a reservoir represents a mesoscopic or, alternatively, a semi-classical spacetime

Table 1. Summary of the simulations

Model	N_v	N_{steps}	Color Increments ($\mathcal{C}_A, \mathcal{C}_B$ or \mathcal{C}_C)	N_{RUNS}
A ($\Delta c_{k+1} = \Delta c_k + \mathcal{C}_A$)	484	10^5	$\{2, 20, 200\}$	$\{5, 5, 5\}$
		10^6	$\{2, 20, 200\}$	$\{5, 5, 5\}$
		10^7	$\{2, 20, 200\}$	$\{1, 1, 1\}$
	3136	10^5	$\{2, 200\}$	$\{1, 1\}$
		10^7	$\{2, 200\}$	$\{1, 1\}$
B ($\Delta c_{k+1} = \Delta c_k + \text{Rand}(2, \mathcal{C}_B)$)	484	10^5	$\{4, 20, 200\}$	$\{5, 5, 5\}$
		10^6	$\{4, 20, 200\}$	$\{5, 5, 5\}$
		10^7	$\{4, 20, 200\}$	$\{1, 1, 1\}$
	3136	10^5	$\{4, 200\}$	$\{1, 1\}$
		10^7	$\{4, 200\}$	$\{1, 1\}$
C ($\Delta c_{k+1} = \Delta c_k + \mathcal{C}_C[f(k)]$)	484	10^5	$\{2, 20, 200\}$	$\{5, 5, 5\}$
		10^6	$\{2, 20, 200\}$	$\{5, 5, 5\}$
		10^7	$\{2, 20, 200\}$	$\{1, 1, 1\}$
	3136	10^5	$\{2, 200\}$	$\{1, 1\}$
		10^7	$\{2, 200\}$	$\{1, 1\}$
Ans08 ($\Delta c_k = 2$; fixed)	484	10^5	0	5
		10^6	0	5
		10^7	0	1
	3136	10^5	0	1
	3136	10^7	0	1

region, from which it can be affected and affect the TSNs. Hence, one may consider that the externally induced disturbances may change not only at random intervals but also in scale, for instance, as a backreaction mechanism. In this sense, perturbations of the TSN and the background reservoir could be correlated with a hybrid scheme [19], a line of investigation which is being currently studied, but which is outside the scope of the present paper.

3.3. Simulations.

We developed a `Python` [20] code (with the `SciPy` [21] package for curve fitting) to implement the algorithms related to the TSN construction, edge color attribution, gauge-invariant tests, propagation rules (the simulations *per se*) and analysis of the results. Our set of simulations incorporate the new propagation rules given by the models, A, B and C, described in the previous section, and also the Ans08 Model, giving a total of 124 simulations. The list of simulations and general parameters are summarized in Table 1, with a few observations, as follows:

- The size of the TSN, given by the total number of vertices (N_v): our simulations were run for both the options $N_v = \{484, 3136\}$. Note: [Ans08] used $N_v = 361$,

whereas [Che08] used $N_v = 10000$ (they also explored a range of N_v values as a check of the results found in [Ans08]).

- The number of activation steps, chosen from the options $N_{\text{steps}} = \{10^5, 10^6, 10^7\}$.
- The color increments, as specified in the previous section. We use the notation $\mathcal{C} \equiv \{\mathcal{C}_A, \mathcal{C}_B, \mathcal{C}_C\}$, as a proxy for any of the color increments used in these models. Hence, the minimum color increment used was $\mathcal{C} = 2$, and the maximum was $\mathcal{C} = 200$. These color increments result in cumulatively large values of the color perturbation Δc as the number of steps is increased, as will be discussed in the next section. Note that $\mathcal{C} = 0$, for the [Ans08] model, as the color perturbation was fixed to $\Delta c_k = 2$ (i.e., no color increment scheme was imposed).
- Number of runs (N_{RUNS}) of a given type of simulation, i.e., using the same parameters, but starting from a different (new realization) of initial conditions on the edge colors as well as from a new random selection of activation vertices. Note that initial colors are randomly chosen from integers in the set $\mathcal{C}_{\text{init}} = \{10, \dots, 30\}$ (even), as in [Ans08], under the condition of a global gauge-invariance on the TSN.

The largest TSN runs ($N_v = 3136$, $N_{\text{steps}} = 10^7$) were computationally very demanding for our current resources, and under our specific `Python` implementation. Hence, we explored a smaller set of the parameters for these runs, and did not perform additional realizations (for the same parameters), as were done for the smaller TSN runs (c.f. N_{RUNS} column in Tab.1).

4. Results

4.1. Avalanches.

We fitted our models to the Pareto distribution, Eq. 3; however, we tested for other heavy-tailed distributions, such as the log-normal and log-Cauchy distributions [13], obtaining worse or sometimes non-convergent fits. The Pareto distribution was adequate in fitting all our models, resulting in different values of the exponent α , all within the range $\alpha \in [-3.23, -2.41]$ (to be discussed in more detail in the next subsection). That is, despite the difference in the color increment rules (fixing all the other parameters), all models follow a similar scale invariant behavior, indicative of SOC.

We present the avalanche results of our A, B and C models, for $N_{\text{steps}} = 10^7$, in Fig. 1, for TSN sizes of $N_v = 484$ (top panel) and $N_v = 3136$ (bottom panel), respectively. The corresponding results for the (single) Ans08 run are displayed in the same graphs for comparison. In order to avoid excessive clutter in our presentation, we only display here the results for $N_{\text{steps}} = 10^7$, leaving a presentation of the other runs in Appendix A. The panels of Fig. 1 show log-log plots of the probability distribution function of avalanches, in terms of avalanche sizes, $\mathcal{P}(s)$ and areas. We include two lines ($\alpha = -3.70$ and $\alpha = -2.80$) for reference only. Stacked areas are also shown, with a behavior qualitatively also similar to those found in [Ans08] (see their Fig. 5).

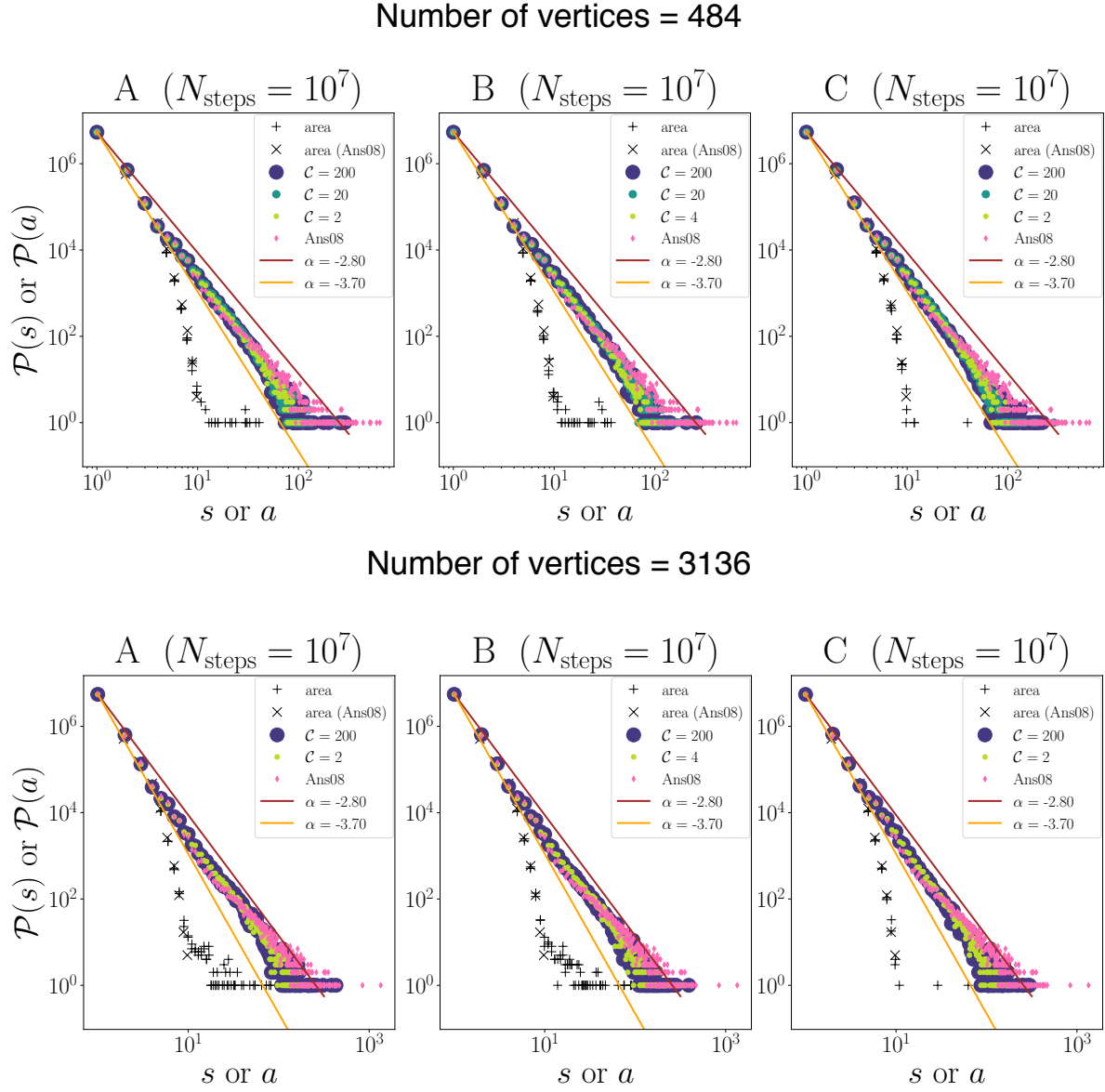


Figure 1. Log-log plots of the distribution of avalanche sizes (circles) and areas (crosses and pluses) for the A, B and C models, with the (single) Ans08 run also displayed in each of these panels for comparison; results are for the $N_{\text{steps}} = 10^7$ runs only (c.f. Tab. 1). Circular symbol sizes are proportional to the color increment \mathcal{C} used. *Top:* $N_v = 484$; *bottom:* $N_v = 3136$. Lines ($\alpha = -3.70$ and $\alpha = -2.80$) are for reference only.

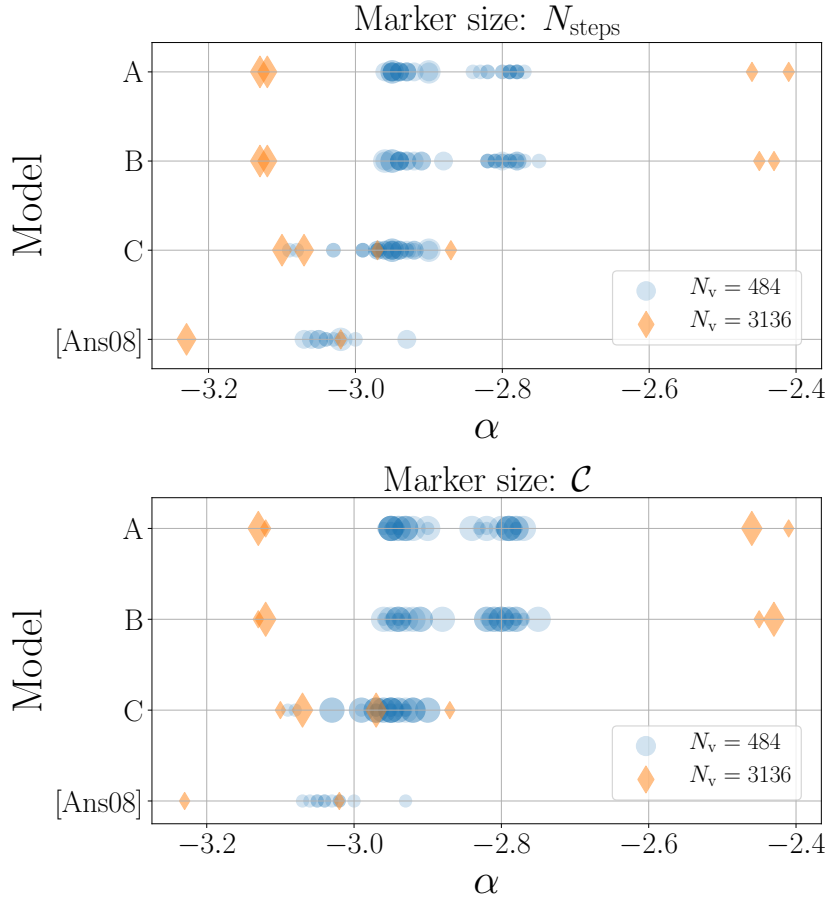


Figure 2. Pareto best-fitting α values ($P(s) = s^\alpha, \alpha < 0$) for all simulations in this work (c.f. Tab. 1), as a function of the size of the TSN (circles: $N_v = 484$; diamonds: $N_v = 3136$). Results are displayed such that the marker (symbol) sizes are proportional to N_{steps} (top panel) and to color increment \mathcal{C} (bottom panel).

We confirm the evidence of SOC in the Ans08 model, here analyzed using larger sizes for the TSN and evolving the disturbances for three ranges of N_{steps} (c.f. Tab. 1). In [Ans08], the best-fitting parameter has been originally found to be: $\alpha = -3.3$ for $N_{\text{steps}} = 10^7$. We confirm a close value, of $\alpha = -3.23$, for the run $N_v = 3136$, $N_{\text{steps}} = 10^7$ (whereas advancing less steps, i.e., for $N_{\text{steps}} = 10^5$, we found $\alpha = -3.02$; see next subsection for more details).

4.2. Behavior of the α exponent.

We present in Fig. 2 a summary of the fittings to the log-log plots of the probability distribution function of avalanches, in terms of avalanche sizes, for all simulations in the present work (c.f. Tab. 1 and Appendix A). For each model, the Pareto α values are shown as a function of the size of the TSN, and also as a function of N_{steps} and color increment \mathcal{C} (see the corresponding caption for further details). We note the following general trends:

- The overall behavior of the α exponent seems to be highly sensitive to N_{steps} in the case of the larger TSN runs ($N_v = 3136$), as compared to the smaller TSN runs ($N_v = 484$). In the former case, fewer number of steps (less evolution) result in significant shallower distributions (specially for the A and B models, giving $\alpha > -2.5$), whereas the latter cases result in larger $|\alpha|$ values. The C models, however, show less sensitivity to N_{steps} as compared to the other models.
- The resulting α exponent seems somewhat insensitive to the color increment used, for any fixed model.
- The A and B models show very similar results. The C and Ans08 models show a slight tendency for larger $|\alpha|$ values than the A and B models, for the smaller TSN runs.

4.3. Mean color evolution.

In Fig. 3, we present the mean color evolution of the whole TSN, $\langle c \rangle$, for the largest TSN ($N_v = 3136$), where the mean color is calculated at each step of the dynamics imposed by the propagation rules of the models. The plots show the evolution up to $N_{\text{steps}} = 10^7$, with the results for $N_{\text{steps}} = 10^5$ also shown (which were run independently, c.f. Tab. 1). Insets show the respective evolutions in a log-log scale.

Given the scales involved, the mean color evolutions of the $N_{\text{steps}} = 10^5$ runs closely overlap those at the initial stages of the $N_{\text{steps}} = 10^7$ runs, at the resolution of the graphs. Although they actually statistically disperse, the effect is not significant initially. However, as the evolution proceeds, the outcomes begin to disperse even more. In the Appendix A, the corresponding figures for the smaller TSN ($N_v = 484$) runs give an indication of the statistical dispersion of these curves, c.f. Figs. A3 and A4. It is also clear that the mean color evolution of the larger TSN is much less noisy than those of the smaller TSN runs, a result also found by [Che08].

We highlight a few observations on the mean color evolution of the present models:

- Clearly, the new models (A, B, C) produce very high mean TSN color values after a certain amount of steps. For models with the smallest color increments (C), the final mean color value reaches $\langle c \rangle_{(10^7)} \sim 10^9$; whereas for the largest color increment, $\langle c \rangle_{(10^7)} \sim 10^{11}$. This is to be contrasted with the much smaller values obtained in the Ans08 model, as expected (i.e., no color increment prescription besides the fixed color perturbation $\Delta c_s = 2$).
- The high values of $\langle c \rangle$ were expected, but the form of those curves were not exactly inferred beforehand. *A posteriori*, we noted that the A and B models behave very similarly, following an approximately straight line in the log-log plots (insets), which indicates that $\langle c \rangle$ follows a power law relationship with the number of steps. The C models resemble the Ans08 model in the sense that the increase of $\langle c \rangle$ is initially small, but amplifies after $\sim 10^4$ steps. However, the Ans08 model subsequently follows an approximately straight line in the log-log scale plot, whereas the C model

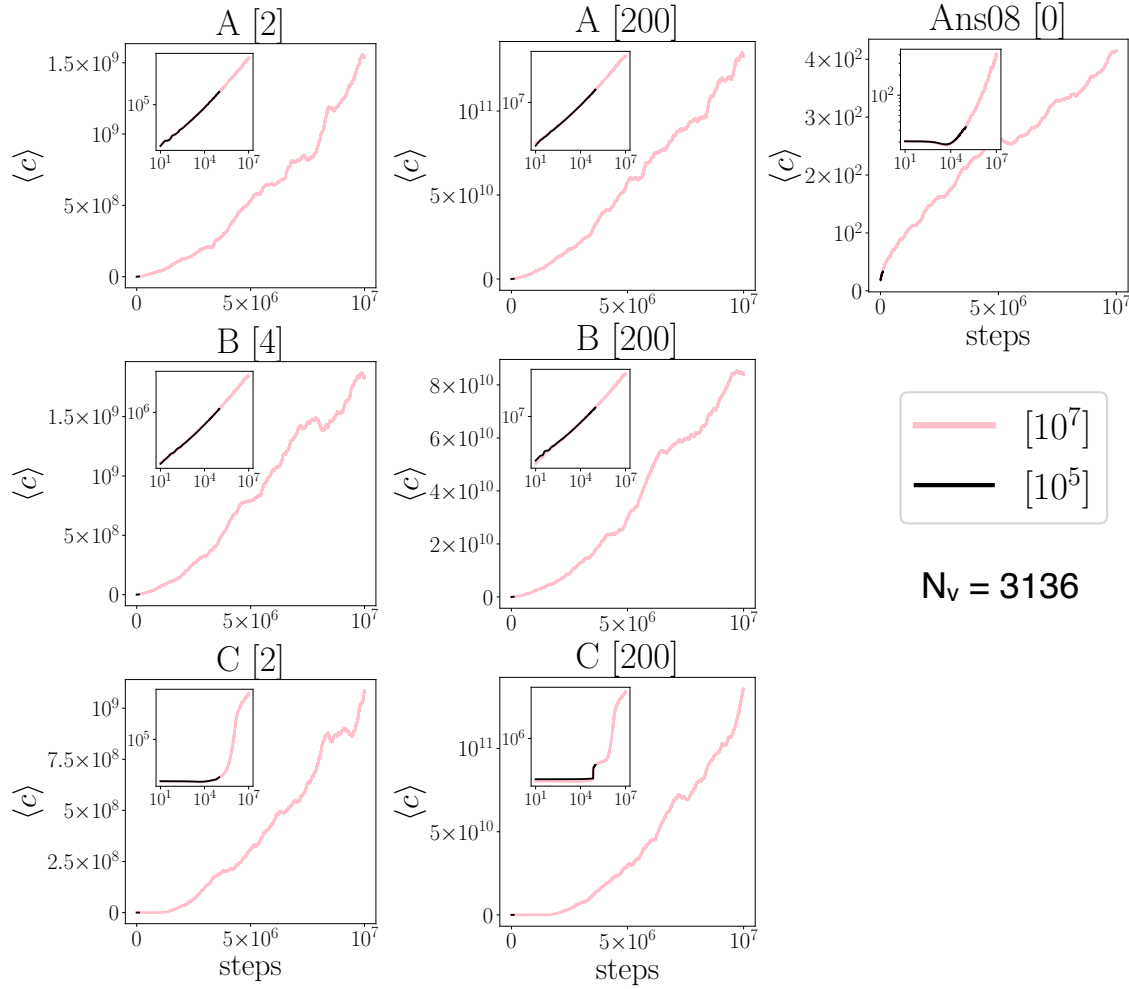


Figure 3. Mean color ($\langle c \rangle$) evolution of the TSN with $N_v = 3136$, for each model, and for the color increment \mathcal{C} specified in brackets next to the model label; log-log scale plots are shown in the respective insets. The evolution of $\langle c \rangle$ is shown for independent simulations, each run up to $N_{\text{steps}} = 10^5$ and $N_{\text{steps}} = 10^7$ (plotted in the same respective panels).

increases steeply, and with a more complicated evolution, nevertheless, showing a behavior consistent with the growth scheme for this model.

5. Summary and conclusions

This work revisited the simulations of frozen TSN dynamics based on LQG concepts [16], [17], as part of an ongoing investigation of the hypothesis that classical spacetime could emerge from a quantum geometric background, based on an underlying self-organized critical (SOC) process.

We expanded the previous work by providing new propagation rules with a growth scheme for the frozen TSN model, which did not follow the sandpile model, that is, we investigated the possibility of a stronger and systematic external driving force, as a

backreaction model. Our new models closely generated power-law distributed avalanche sizes (SOC), while showing a significantly pronounced increase of the mean color of the TSN with time (here understood as an external variable parameterizing the agency of sequential, stochastic disturbances).

The resulting expanding dual spaces showed two basic classes of evolution: one with power-law correlations in space and time, and the other with “loitering” and exponential phases. Our work expanded the range of models in which critical states in the TSN could lead to expansion effects in the dual space, without fine-tuning. Further exploration of those models could provide interesting signatures in a quantum cosmology context, specially when considering the possibility that signature changes and/or phase-transitions may occur in the gravitational sector in the early Universe (e.g. [22], [23] and references therein).

It is not certain whether the statistical outcomes of the models studied here represent a robust, emergent feature of quantum spacetime, whose microscopic behavior is still unknown. It is, however, possible that spontaneously occurring critical states are a natural phenomenon in LQG. Under this hypothesis, simulations exploring criticality become complementary to detailed computations of LQG states, and could provide further hints on an intermediate or mesoscopic point of view concerning the transition to the classical spacetime limit.

A connection of the point of view above with hybrid schemes in quantum cosmology [19] would be very interesting. Another potentially fruitful connection arises from recent numerical results [24], in which large variances in geometric variables were found in a LQG computation, with stochastic correlations that suggest an alternative model to inflation. It would be interesting to address the behavior of this class of LQG models in the present context of criticality.

Appendix A. Supplementary results for the smaller TSN ($N_v = 484$)

In this appendix, we present the complete set of graphics related to the distribution of avalanches and mean color evolutions, for the $N_v = 484$ runs, which were omitted in the main text for clarity. In the case of avalanche graphs for $N_{\text{steps}} = 10^7$, the results for this smaller TSN were already shown in the main text (Fig. 1). Here, we present the supplementary results and briefly discuss them.

In the case of avalanches, for $N_{\text{steps}} = \{10^5, 10^6\}$, $N_v = 484$, Figs. A1 and A2 show the results for the A, B and C models and for the Ans08 model, respectively. Clearly, all models show evidence for power-law distributed avalanche sizes (SOC), even considering that these models were run on a smaller TSN and for shorter number of steps, as compared to runs using the larger TSN ($N_v = 3136$), up to $N_{\text{steps}} = 10^7$; c.f. Fig. 1.

In Figs. A3 and A4, we present the mean color evolution of the TSN, for different time scales, respectively, for up to $N_{\text{steps}} = 10^6$, and up to $N_{\text{steps}} = 10^7$, in order to better visualize the graphics in these different phases. Note that these cases were run independently, forming therefore an ensemble of different realizations of the same models, from different initial conditions, and evolving up to the corresponding N_{steps} (c.f. Tab 1).

As mentioned in the main text, the results for the smaller TSN showed a more noisy $\langle c \rangle$ evolution, than using the TSN with $N_v = 3136$ (c.f. Fig. 3), in agreement with [Che08]. We also noted that, using the smaller TSN, all models, including the Ans08 model, present a considerable amplification of the noise for larger time scales (i.e., steps greater than $\sim 10^6$). The qualitative form of the mean color evolution also presents a more complicated behavior at these larger time scales than in the initial steps.

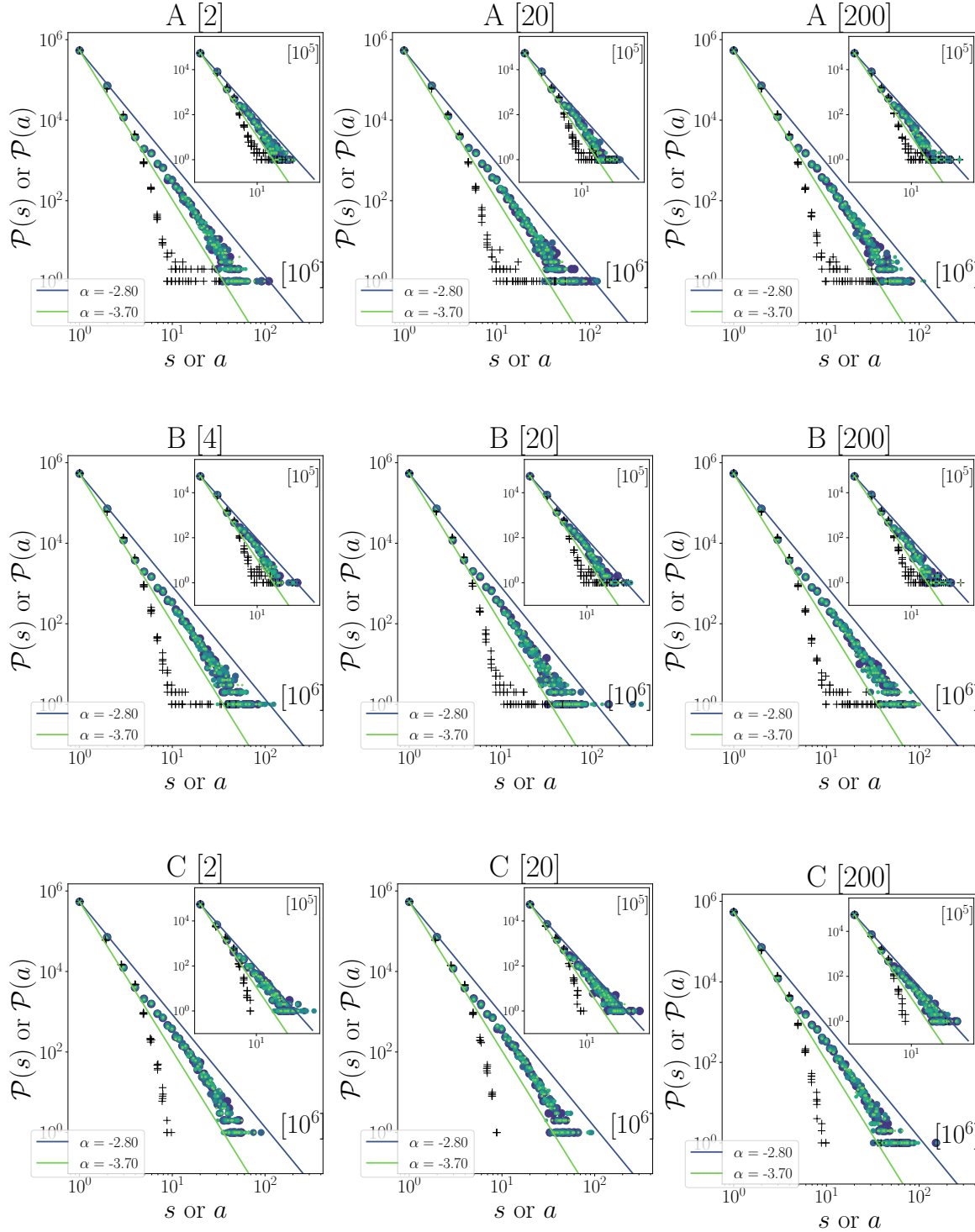


Figure A1. Log-log plots of the distribution of (stacked) avalanche sizes (circles) and areas (pluses) for the A, B and C models in the smaller TSN ($N_v = 484$). Color increment (C) is specified in brackets next to the model label. Results are for the $N_{\text{steps}} = 10^6$ (main panels) and $N_{\text{steps}} = 10^5$ (insets); c.f. Tab. 1. Each of these models had 5 independent runs, stacked in the same respective panels, with different marker colors. Lines ($\alpha = -3.70$ and $\alpha = -2.80$) are for reference only.

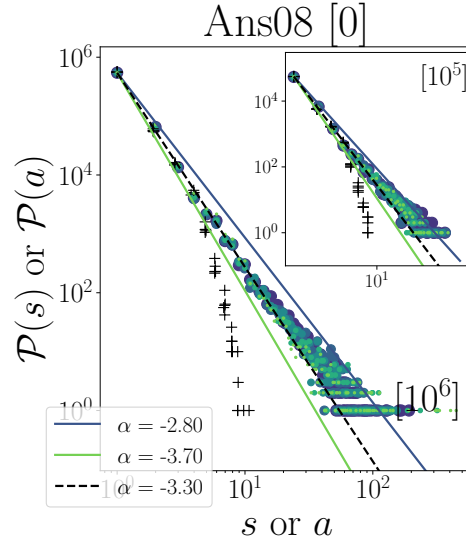


Figure A2. Same as the previous figure, for the Ans08 model only ($N_v = 484$). Black dashed line shows the best-fitting of α found in [Ans08].

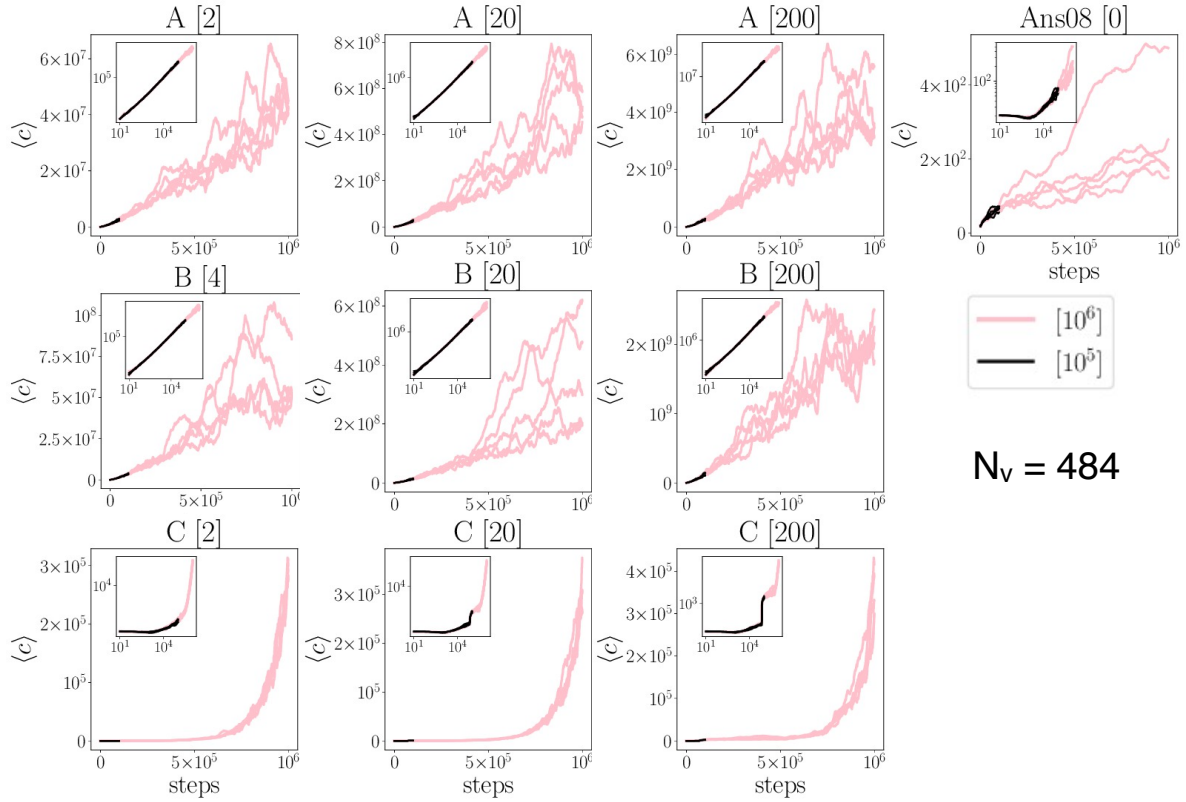


Figure A3. Mean color ($\langle c \rangle$) evolution of the TSN with $N_v = 484$, for each model, and for the color increment \mathcal{C} specified in brackets next to the model label; log-log scale plots are shown in the respective insets. The evolution of $\langle c \rangle$ is shown for independent simulations, each run up to $N_{\text{steps}} = 10^5$ and $N_{\text{steps}} = 10^6$ (plotted in the same respective panels).

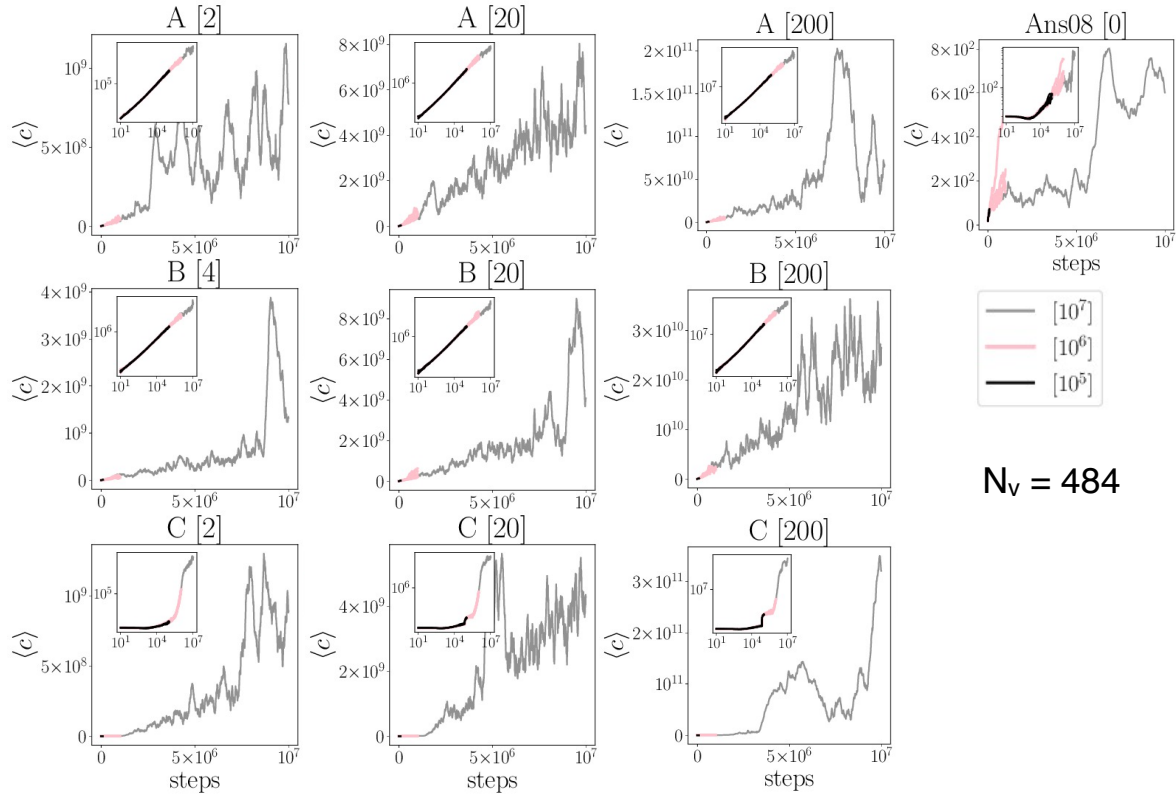


Figure A4. Same as the previous figure, but including simulations run up to $N_{\text{steps}} = 10^7$.

References

- [1] Rovelli C 1998 *Living Reviews in Relativity* **1** URL <https://doi.org/10.12942/lrr-1998-1>
- [2] Rovelli C 2007 *Quantum Gravity* Cambridge Monographs on Mathematical Physics (Cambridge University Press) ISBN 978-0521715966
- [3] Thiemann T 2008 *Modern Canonical Quantum General Relativity* Cambridge Monographs on Mathematical Physics (Cambridge University Press) ISBN 978-0521741873
- [4] Rovelli C and Vidotto F 2020 *Covariant Loop Quantum Gravity* (Cambridge University Press) ISBN 978-1108810258
- [5] Smolin L 2005 *arXiv e-prints* hep-th/0507235 (Preprint [hep-th/0507235](https://arxiv.org/abs/hep-th/0507235))
- [6] Penrose R 1971 *Angular momentum: an approach to combinatorial space-time* (Cambridge University Press) pp 151–180 URL <https://math.ucr.edu/home/baez/penrose/>
- [7] Smolin L 2004 An Invitation to Loop Quantum Gravity *Quantum Theory and Symmetries* pp 655–682 (Preprint [hep-th/0408048](https://arxiv.org/abs/hep-th/0408048))
- [8] Baez J C 2000 *An Introduction to Spin Foam Models of BF Theory and Quantum Gravity (Lecture Notes in Physics vol 543)* (Springer, Berlin, Heidelberg) p 25 ISBN 978-3-662-14287-5
- [9] Markopoulou F and Smolin L 1997 *Nuclear Physics B* **508** 409–430 (Preprint [gr-qc/9702025](https://arxiv.org/abs/gr-qc/9702025))
- [10] Bak P, Tang C and Wiesenfeld K 1987 *Phys. Rev. Lett.* **59**(4) 381–384 URL <https://link.aps.org/doi/10.1103/PhysRevLett.59.381>
- [11] Bak P, Tang C and Wiesenfeld K 1988 *Phys. Rev. A* **38**(1) 364–374 URL <https://link.aps.org/doi/10.1103/PhysRevA.38.364>
- [12] Dhar D 1990 *Phys. Rev. Lett.* **64**(14) 1613–1616 URL <https://link.aps.org/doi/10.1103/PhysRevLett.64.1613>
- [13] Marković D and Gros C 2014 *Phys. Rep.* **536** 41–74 (Preprint [1310.5527](https://arxiv.org/abs/1310.5527))
- [14] Watkins N W, Pruessner G, Chapman S C, Crosby N B and Jensen H J 2016 *Space Sci. Rev.* **198** 3–44 (Preprint [1504.04991](https://arxiv.org/abs/1504.04991))
- [15] Borissov R and Gupta S 1999 *PRD* **60** 024002 (Preprint [gr-qc/9810024](https://arxiv.org/abs/gr-qc/9810024))
- [16] Ansari M H and Smolin L 2008 *Classical and Quantum Gravity* **25** 095016 (Preprint <https://arxiv.org/abs/hep-th/0412307>)
- [17] Chen J Z and Zhu J Y 2008 *International Journal of Modern Physics A* **23** 3891–3899 (Preprint <https://arxiv.org/abs/gr-qc/0701175>)
- [18] Kuchař K V 2011 *International Journal of Modern Physics D* **20** 3–86
- [19] Bojowald M and Ding D 2021 *Journal of Cosmology and Astroparticle Physics* **2021** 083 (Preprint [2011.03018](https://arxiv.org/abs/2011.03018))
- [20] Foundation P S 2019 Python language reference, version 3.7.6 URL <http://www.python.org>
- [21] Virtanen P, Gommers R, Oliphant T E, Haberland M, Reddy T, Cournapeau D, Burovski E, Peterson P, Weckesser W, Bright J, van der Walt S J, Brett M, Wilson J, Millman K J, Mayorov N, Nelson A R J, Jones E, Kern R, Larson E, Carey C J, Polat İ, Feng Y, Moore E W, VanderPlas J, Laxalde D, Perktold J, Cimrman R, Henriksen I, Quintero E A, Harris C R, Archibald A M, Ribeiro A H, Pedregosa F, van Mulbregt P and SciPy 10 Contributors 2020 *Nature Methods* **17** 261–272
- [22] Bojowald M and Mielczarek J 2015 *Journal of Cosmology and Astroparticle Physics* **2015** 052 (Preprint [1503.09154](https://arxiv.org/abs/1503.09154))
- [23] Mielczarek J 2014 *arXiv e-prints* arXiv:1404.0228 (Preprint <https://arxiv.org/abs/1404.0228>)
- [24] Gozzini F and Vidotto F 2021 *Frontiers in Astronomy and Space Sciences* **7** 118